Structure and Evolution of Winter Cyclones in the Central United States and Their Effects on the Distribution of Precipitation. Part V: Thermodynamic and Dual-Doppler Radar Analysis of a Squall Line Associated with a Cold Front Aloft

JOHN D. LOCATELLI, MARK T. STOELINGA, AND PETER V. HOBBS

Department of Atmospheric Sciences, University of Washington, Seattle, Washington

(Manuscript received 18 April 1997, in final form 12 September 1997)

ABSTRACT

On 8–9 March 1992, a long-lived squall line traversed the state of Kansas, producing hail and damaging winds. It was shown previously that this squall line was part of a synoptic-scale rainband 2000 km in length that was associated with a cold front aloft (CFA). The present study is concerned with the detailed mesoscale structure of this squall line and its relationship to the CFA.

Examination of synoptic-scale cross sections based on rawinsonde ascents, and a mesoscale cross section of winds derived from dual-Doppler radar measurements, shows that the squall line was exactly coincident with the ''nose'' of the CFA. The dual-Doppler analysis also shows that the inflow of air to the squall line was elevated, drawing in air from the potentially unstable layer within the weak warm frontal–like feature that was being occluded by the CFA. The stability analysis of the air in the pre-squall-line environment shows that when the CFA overtook the surface position of the drytrough, the thermal and moisture structure of the atmosphere was such that a moderate amount of lifting provided by the CFA could have released convective instability within an elevated layer approximately 1–2 km above ground.

The mesoscale structure of the squall line, derived from the radar reflectivity and dual-Doppler wind fields, differs substantially from the ''leading line/trailing stratiform'' conceptual model for midlatitude squall lines. The lack of a strong cold pool, and the presence of strong low-level shear, indicates that the squall line described here was able to persist in its mature stage in an environment that was ''greater than optimal'' in terms of the balance of the vorticity of the cold pool to that of the low-level shear. However, in view of 1) the weakness of the surface cold pool, 2) the elevated inflow and convergence associated with the convection, and 3) the collocation of the large rainband in which the squall line was embedded and the CFA, it seems likely that the CFA (rather than the cold pool) provided the driving force for the squall line.

1. Introduction

Locatelli et al. (1995) analyzed a rainband that consisted of a series of long-lived squall lines, which extended in an approximately 1000-km-long arc over the central United States on 8–9 March 1992. This rainband was shown to be coincident with a cold front aloft (CFA) throughout its life cycle, and was therefore termed a *CFA rainband.* The CFA was part of a warm-occluded-like structure that commonly occurs in the southeastern quadrant of cyclones in the central United States, as depicted in the Structurally Transformed by Orography Model, STORM (Hobbs et al. 1996). In this paper, we focus on a particular segment of the 8–9 March 1992 CFA rainband, namely, a squall line that traversed the state of Kansas. The purpose of this study is to gain a clearer understanding of the mesoscale structure of the squall line and its relationship to the CFA.

The CFA rainband occurred during an intensive observation period of the Storm-scale Operational and Research Meteorology–Fronts Experiment Systems Test (STORM-FEST) field program, which took place in the central United States from 1 February to 15 March 1992. The squall line and its environment were probed in detail by three-hourly soundings, Portable Automated Mesonet (PAM) surface observations, and dual-Doppler radars. In this paper we use these data for reflectivity and dual-Doppler velocity analyses, stability analyses of the pre-squall-line environment, and analysis of the vertical structure of the squall line.

The results presented here demonstrate the collocation of the squall line and the CFA with significantly greater precision than is possible with the conventional upper-air data used by Locatelli et al. (1995). The surface, upper-air, and dual-Doppler observations are also used to compare the squall line to other midlatitude squall lines that have been documented, to the Houze et al. (1989) ''leading line/trailing stratiform'' conceptual model for midlatitude squall lines, and to recent

Corresponding author address: Peter V. Hobbs, Department of Atmospheric Sciences, University of Washington, Box 351640, Seattle, WA 98195-1640.
E-mail: phobbs@atmos.washington.edu

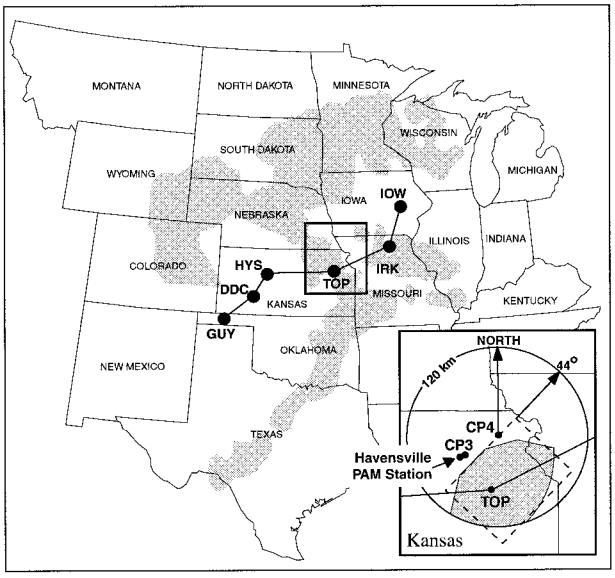

FIG. 1. The central United States showing the location of the cross sections discussed (circles connected by the heavy solid line) and the location of the surface stations [Guymon, Oklahoma (GUY); Dodge City, Kansas (DDC); Hays, Kansas (HAY); Topeka, Kansas (TOP); Kirksville, Missouri (IRK); and Iowa City, Iowa (IOW)] from which 3-h rawinsondes were launched. The gray shading shows the area covered by the lowest-intensity radar echoes from the national radar summary valid at 0635 UTC 9 March 1992. The insert is an enlargement of the box around Topeka, Kansas (TOP) showing the location of the CP4 and CP3 dual-Doppler radar pair, the 120-km range of the CP4 radar, the region where dual-Doppler data was obtained (shaded area), and the rectangle in which the dual-Doppler data will be shown (dashed box).

theoretical ideas that relate environmental parameters to squall-line structure (e.g., Rotunno et al. 1988).

2. Overview and cross-sectional analysis of the squall line

Figure 1 shows the location of a series of cross sections through the squall line. These cross sections are based on data from 3-h rawinsonde ascents from the six stations shown in Fig. 1. The radar echoes shown in Fig. 1, which are for 0635 UTC 9 March 1992, show the CFA rainband extending as an arc through Nebraska, Kansas, Oklahoma, and Texas.

Figure 2 shows digitized National Weather Service (NWS) radar echoes that reveal the location and intensity of the precipitation associated with the squall line as it traversed the state of Kansas. At 0000 UTC 9 March 1992 (Fig. 2a), the ''drytrough'' [i.e., a trough with the characteristics of a lee trough and a dryline (Martin et al. 1995)] was located between Guymon, Oklahoma (GUY), and Dodge City, Kansas (DDC). Weak scattered radar echoes were located west of the drytrough, and isolated stronger echoes to the east of the drytrough. Between 0000 and 0145 UTC 9 March (Fig. 2b), a line of radar echoes developed west of DDC. As this line moved eastward and away from the drytrough, it increased in length. At 0300 UTC 9 March, when the squall line was located between DDC and Hays, Kansas (HYS, Fig. 2c), there were reports from near the southern end of the squall line of 1-in. hail, downed power lines, and a destroyed shed, which gives some indication of the severity of the convective storm at this time. Three hours later, at 0600 UTC 9 March (Fig. 2d), an F0 tornado [see Fujita (1981) for a description of the F scale] and 1-in. hail were reported in Butler County, Kansas, which was located near the southern end of the squall line. From 0600 to 1200 UTC 9 March, the squall line continued to move eastward away from the drytrough (Figs. 2e,f). As the squall line increased in size, the isolated radar echoes ahead of it also increased in size, but they dissipated as the squall line approached. The isolated radar echoes located behind the squall line dissipated during these same time periods. These figures show only a portion of the squall lines that comprised the CFA rainband [see Fig. 5 of Locatelli et al. (1995) for a larger-scale view of this rainband].

Cross sections every 3 h of temperature and equivalent potential temperature θ_e along the line shown in Fig. 1 from GUY to Iowa City, Iowa (IOW), are shown in Fig. 3. The times listed are for the launch times rounded to the nearest whole hour. All the soundings were generally started within 10 min of the hour, except for a few soundings that were started about 30 min after the hour. The time and space scales are large enough in the cross section that this time difference is not important. The positions of the squall line, taken from the maps of radar echoes in Fig. 2, are marked by the vertical rectangle labeled SL in Fig. 3. A tongue of high-θ_e air, extending upward and eastward from the drytrough, can be seen in each cross section in Fig. 3. This is the result of a weak warm frontal–like circulation, associated with the drytrough, that lifted high-θ_e air from the Gulf of Mexico out and away from the drytrough, in a slantwise zone. Above this tongue is a region of dry, low-θ_e air that recently descended from the Rocky Mountains (Martin et al. 1995). At 0200 UTC 9 March, the squall line was directly over DDC. It appears that the rawinsonde ascended into the squall line itself, as can be seen from the narrow region of higher θ_e air and higher temperatures aloft over DDC. In this figure, as in Fig. 2, the squall line is seen to move eastward, away from the drytrough. As deduced by Locatelli et al. (1995), Fig. 3 shows that the squall line developed when the CFA reached the vicinity of the drytrough. The CFA was located on the cross sections by taking into account the θ_e and temperature gradients in addition to the vertical wind shear. As the CFA moved eastward over the tongue of high-θ_e air, the squall line also moved eastward, coincident with the nose of the CFA. This warm occlusion-like process is described, through MM4 model simulations, by Castle et al. (1996).

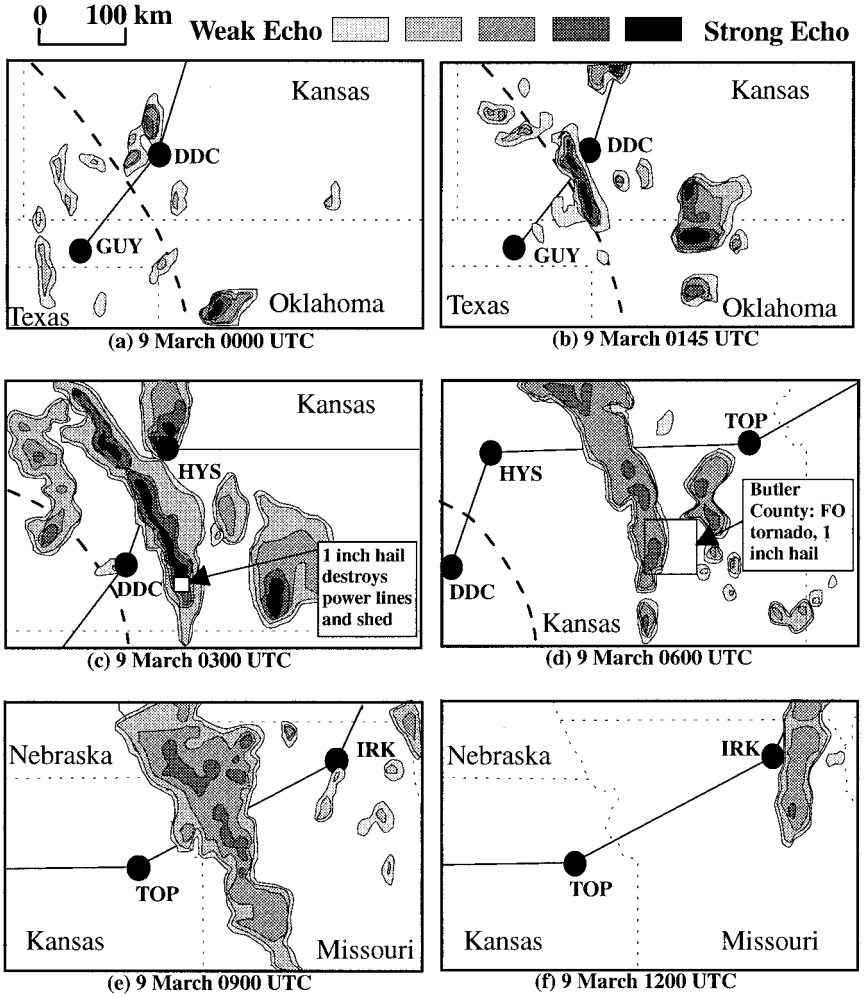

FIG. 2. National Weather Service digitized radar echoes, in relation to the locations of the cross sections shown in Fig. 1, at 0000, 0145, 0300, 0600, 0900, and 1200 UTC 9 March 1992. The inserts indicate damage reported close to the time of the radar echoes.

3. Dual-Doppler analysis

a. Technique

The inset in Fig. 1 shows an enlargement of the region around Topeka, Kansas, where two 5-cm-wavelength Doppler radars (the CP3 and CP4 radars operated by NCAR) were located. The radars, which were on a 52.1-km-long baseline oriented 238° to true north, were operated at a pulse repetition rate of 1080 s^{-1}, which gave a maximum unambiguous range of 139 km and a Nyquist velocity of 14.8 m s^{-1}. During the dual-Doppler mode of operation, both radars made 120° overlapping sector scans. The shaded region in Fig. 1 shows the area of dual-Doppler coverage used in this study. The radial velocities and reflectivities were interpolated to a Cartesian grid with 1.5-km horizontal spacing and 500-m vertical spacing. Details of this process can be found in Mohr et al. (1979), Oye and Carbone (1981), and Mohr and Miller (1983). The location of this grid is shown as a dashed rectangle in the insert to Fig. 1. The *x* axis of the grid (i.e., the long axis of the rectangle) was chosen to be perpendicular to the squall line, and therefore points toward 44° compass direction (i.e., approximately northeast).

b. Radar reflectivity and airflow within the squall line

Figure 4 shows a plan view of radar reflectivity at 1-km elevation, within the region defined by the dashed rectangle in the inset to Fig. 1. In this case, and for all the radar results presented hereafter, the time is 0740 UTC 9 March 1992 (the median time of the period 0738–0742 UTC for the data used in our computations). The squall line is the line of heavier radar echoes located between 75 and 85 km on the *x* axis. Regions of lighter radar echoes can be seen ahead and behind the squall line. The motion of the squall line was determined from two successive horizontal reflectivity scans from the

CP4 radar. The individual cells that comprised the squall line moved toward 44° at 22 m s^{-1}. A transverse cross section of radar reflectivity and winds relative to the motion of the squall line, where both fields are averaged from $y = 45$ to $y = 90$ km, is shown in Fig. 5. Cross sections through each individual cell were also constructed, but were found to be essentially similar to the average cross section shown in Fig. 5. It can be seen from this figure that air converged into the squall line from both ahead of and behind the location of the highest radar reflectivity values (i.e., in the region of heaviest precipitation). The strongest inflow is in an elevated layer between 1 and 4 km. The air ascended in an upright column, with a maximum velocity of 7 m s^{-1}, until it exited the column at an altitude of 7–12 km ahead of the squall line. The lack of a radar bright band in the areas of precipitation ahead of and behind the squall line indicate that these regions were more convective than stratiform. The smaller regions of embedded higher vertical velocity within these areas suggest that the areas of precipitation outside the squall line were also composed of convective cells, though they were considerably weaker than the cells within the squall line.

Figure 6 shows the companion cross section along the y axis, from 25 to 105 km, averaged from $x = 75$ to $x = 85$ km. This figure shows the individual updrafts associated with the cells that comprised the squall line.

Using a variety of cross sections through individual cells and several plan views of the relative winds (not shown), as well as the average cross sections shown in Figs. 5 and 6, a schematic was constructed of the airflow relative to the motion of an individual cell in the squall line (Fig. 7). Relative to the motion of such a cell, the main airflow into the cell is from two airstreams: one from the east and one from the southwest, each located at about 2 km in altitude. These two flows converge on the axis of the squall line, then move upward, slanting to the northwest. At the top of the cell, where the updraft weakens, the airflows turn and flow toward the northeast. Notice that the updrafts are slanted across the regions of falling precipitation (shaded area in Fig. 7), which allows the precipitation to fall between the updraft cores without impeding them.

c. Relationship of the CFA to the squall line

The cross sections shown in Fig. 3 indicate that the squall line developed at or shortly after the time that the CFA overtook the surface position of the drytrough. As the CFA moved over the tongue of high-θ_e air east of the drytrough, the squall line moved away from the drytrough, in the vicinity of the nose of the CFA. Because the cross sections are based on soundings separated by approximately 100–300 km, the cross sections are not accurate enough to pinpoint the exact position of the nose of the CFA relative to the squall line. However, the high-resolution wind data from the dual-Doppler analysis can be used to locate the CFA relative to the squall line to an accuracy of about 5 km. Specifically, the wind direction pattern can be examined to determine regions of vertical wind shear that, from thermal wind balance, indicate the sense of thermal advection. Of course, the feature being examined has a scale for which, strictly speaking, thermal wind balance does not apply. However, since the CFA is a synoptic-scale feature along its length, it is not unreasonable to expect a significant degree of cross-front geostrophy. This contention is supported by the winds at Topeka, shown on the 0800 UTC cross section (Fig. 3d), which display backing of the winds (indicating cold advection) immediately below the CFA and veering of the winds in the warm advection region of the drytrough.

Figure 8a shows a vertical cross section, perpendicular to the squall line and averaged from $y = 0$ to $y = 105$ km, of the horizontal wind vectors. The averaging distance used here was longer than for the cross section shown in Fig. 5, in order to capture the synoptic-scale feature in which the cells were embedded, rather than the airflow within the cells. The position of the squall line is located by the 30-dBZ contour (the shaded region in Fig. 8a). Since the x axis of the cross section is normal to the axis of the squall line, wind vectors that are parallel to the cross section represent southwest winds. The contours of the wind direction are also shown in Fig. 8a; they reveal a definite pattern of cold advection (winds backing with height) overlying warm advection (winds veering with height). The top of the layer of warm advection is marked with a heavy dashed line in Fig. 8 and the leading edge of the region of cold advection by a heavy solid line. The top of the layer of warm advection was located at the top of the zone where the winds changed from veering to backing. The leading edge of the region of cold advection was located at the top of the zone of strongest backing with height. (On Figs. 8b–d, the heavy lines that indicate advection, as well as contours of wind direction, are shown for reference.) Figure 8b shows the interpolated position, derived from cross sections based on serial sondes (Fig. 3), of the tongue of high-θ_e air (light shaded region) and the CFA (darker shading). These features compare well with the advection boundaries derived from the dual-Doppler wind direction analysis, which lends credence to our hypothesis that there existed a sufficient degree of thermal wind balance to allow the vertical wind shear to be used to locate the CFA. Hence, it is concluded that the leading edge of the region of cold advection, as derived from the detailed wind shear, is the CFA; and that the top of the warm advection is the top of the weak warm frontal–like circulation associated with the drytrough.

Other aspects of the squall line can now be related to the position of the CFA. The convergence (averaged over the same region as the winds, and shown in Fig. 8c) is greatest just behind and below the nose of the CFA in the tongue of high-θ_e air, but significant convergence also extends in a column from the boundary

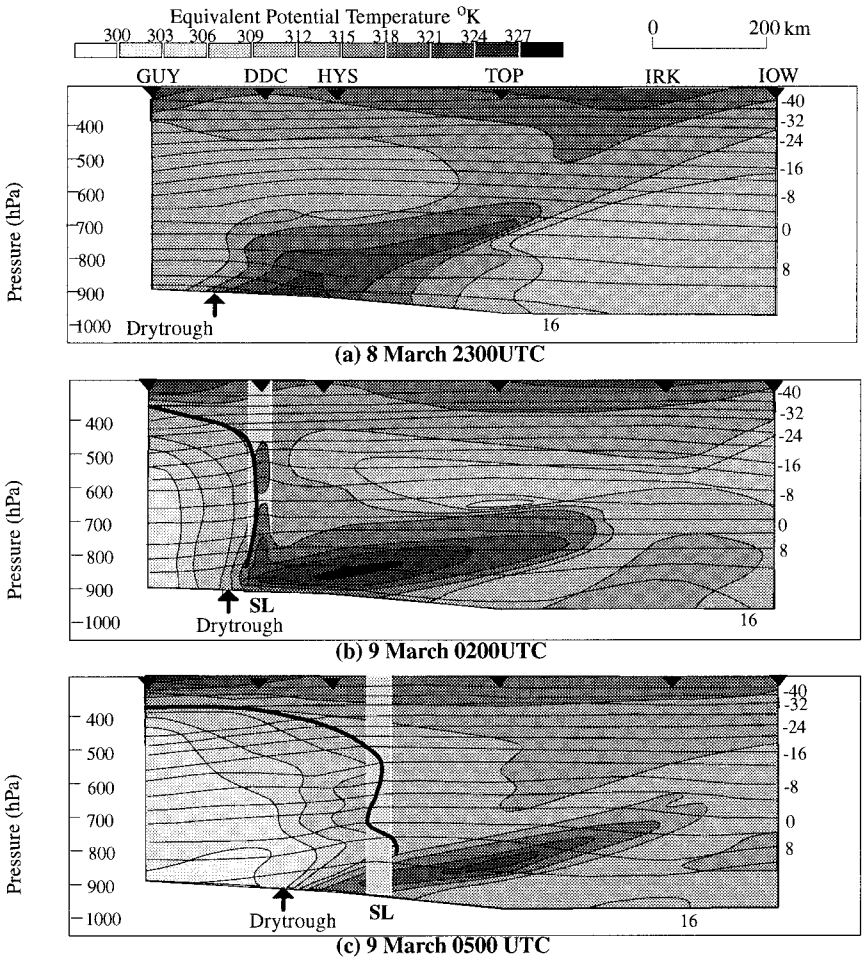

FIG. 3. Cross sections along the lines shown in Fig. 1, from Guymon, Oklahoma (GUY), to Dodge City, Kansas (DDC), Hays, Kansas (HAY), Topeka, Kansas (TOP), Kirksville, Missouri (IRK), and Iowa City, Iowa (IOW), of equivalent potential temperature (contours shaded every 3 K) and temperature (thin lines, shown every 4°C and labeled every 8°C) at 2300 UTC 8 March 1992, and 0200, 0500, 0800, and 1100 UTC 9 March 1992; these times are when the rawinsondes were launched. The location of the squall line at the surface is shown by the lightly shaded vertical rectangle labeled SL. The surface location of the drytrough is shown by the arrow. The black triangles at the top of each cross section indicate the sounding stations used to draw the cross section, and where the data was located in the cross section. Missing triangles indicate that the data were missing for that station at that time. The location of the CFA (defined as the leading edge of the zone of enhanced temperature and θ_e gradient) is shown by the heavy solid line. In (d) the winds at TOP are given by the standard convention.

layer to 500 hPa. The wind vectors relative to the squall line within the plane of the cross section (Fig. 8d) show that the main updraft that fed the squall line was also located just behind the nose of the CFA.

4. Stability of the environment of the squall line

In the two previous sections we have examined the structure of the squall line and its position relative to the surface drytrough and the CFA. Now we examine the environment that the CFA was moving into to determine if the CFA could have provided sufficient lifting to maintain the squall line. Consequently, this section is concerned with the stability of the environment of the squall line, both prior to its initiation and during its mature phase. Whether or not instability is released by lifting depends on two factors: how close air parcels are to their level of free convection (LFC), and the amount of lifting. The first issue can be addressed by examining soundings prior to the initiation of the squall line, which is the main subject of this section.

The second issue is not as straightforward. Locatelli et al. (1995) suggested two mechanisms by which the CFA caused mesoscale ascent in the 8–9 March 1992 case. First, the CFA was characterized by frontogenesis. In two-dimensional theory of balanced frontogenesis,

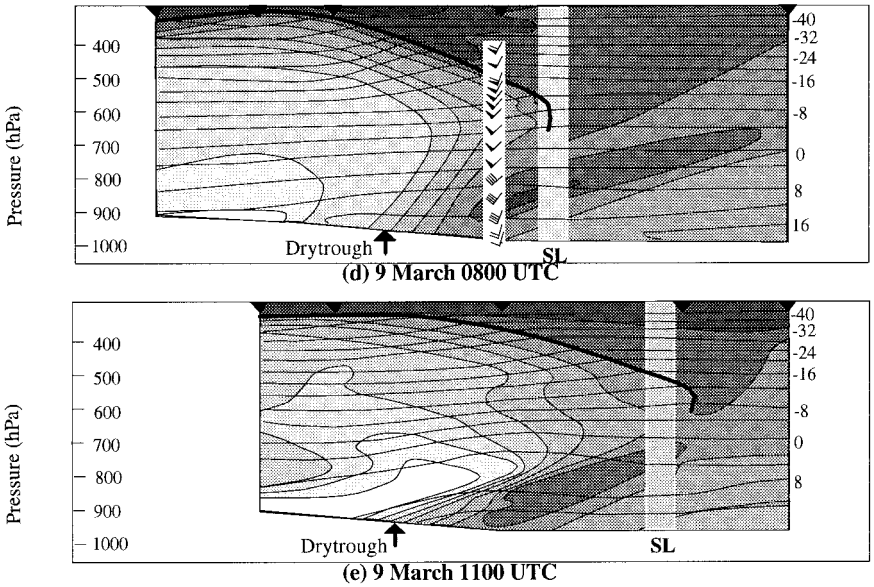

FIG. 3. (*Continued*)

horizontal frontogenesis requires a thermally direct ageostrophic circulation, with ascent on the warm side of the baroclinic zone (Sawyer 1956; Eliassen 1962). This theory can be applied to the midtropospheric baroclinic zone associated with a CFA. If the midtropospheric baroclinic zone is characterized by a frontogenetical horizontal flow, then ascent will occur near the location of the CFA. Locatelli et al. (1995) demonstrated that the CFA in this case was associated with frontogenesis and quasigeostrophic ascent at 2100 UTC 8 March 1992, approximately 10 h prior to the dual-Doppler analysis time. While quasigeostrophic ascent is necessarily a synoptic-scale mechanism, higher-order balance models that include moisture have shown that balanced frontogenetical circulations can act on a much narrower scale (Emanuel 1985). The other mechanism discussed by Locatelli et al. was that a moving CFA within a warm occlusion can induce convergence at low levels in a narrow region located below and behind the nose of the CFA. Simply described, this convergence is a response to the surface isallobaric pattern associated with the CFA passage aloft, although it is not accurately diagnosed with the quasigeostrophic isallobaric wind equation because it is forced by pressure fluctuations that have a subsynoptic (~1 h) timescale (Locatelli et

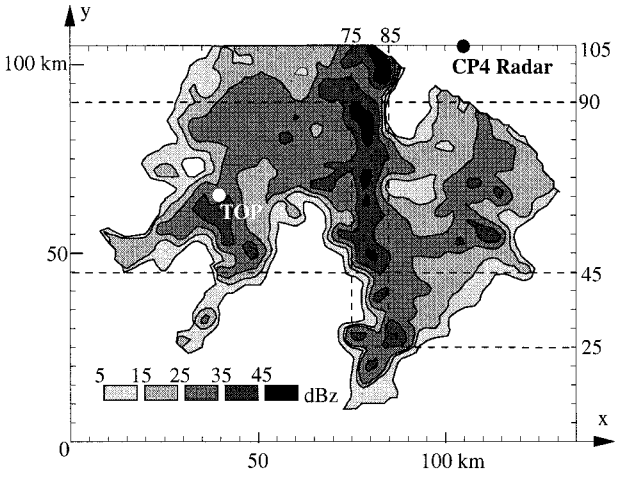

FIG. 4. Radar reflectivities at 1-km elevation at 0740 UTC 9 March 1992. The directions of the *x* and *y* axes are shown by the arrows. The dashed lines indicate the regions over which the vertical cross sections shown in Figs. 5 and 6 are averaged.

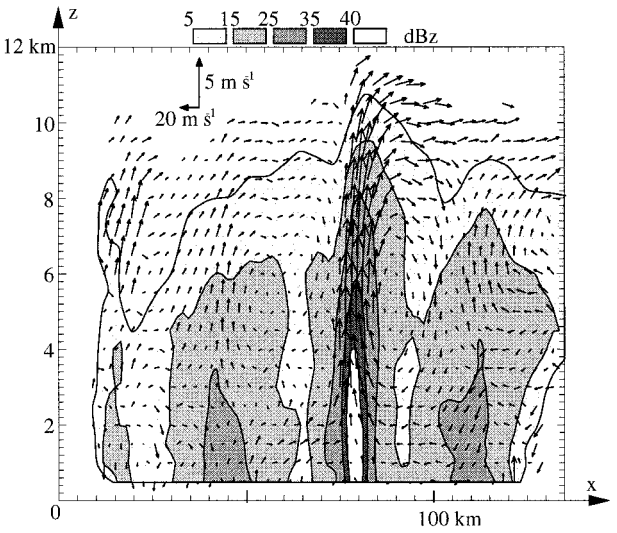

FIG. 5. Radar reflectivities and vector winds in a vertical cross section along the *x* axis from $x = 0$ to $x = 135$ km averaged from $y = 45$ to $y = 90$ km (see Fig. 4).

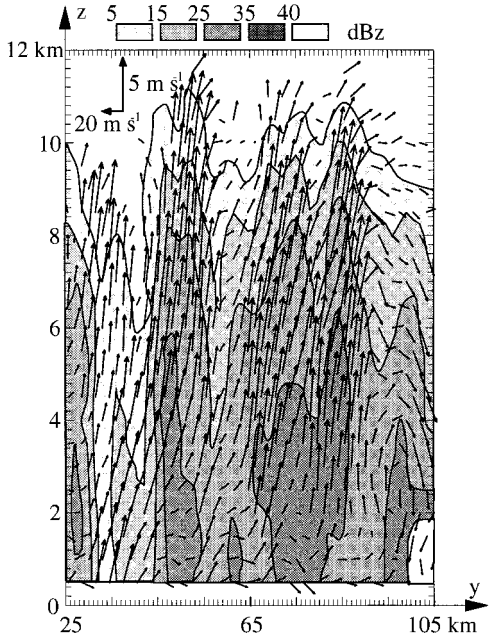

FIG. 6. Radar reflectivities and vector winds in a vertical cross section along the y axis from $y = 25$ to $y = 105$ km average from $x = 75$ to $x = 85$ km (see Fig. 4).

al. 1997). Both mechanisms are qualitatively consistent with the convergence pattern shown in Fig. 8c. However, this convergence pattern includes the buoyancy-driven circulation associated with the mature convective system. Because of the limitations of the data, it is not possible to assess quantitatively the individual contributions of the two proposed CFA-induced lifting mechanisms, and the contribution of the ''self-induced'' buoyancy-driven circulation. In the developing stage of the squall line, the complication of the buoyancy-driven circulation is removed, but no detailed vertical velocity

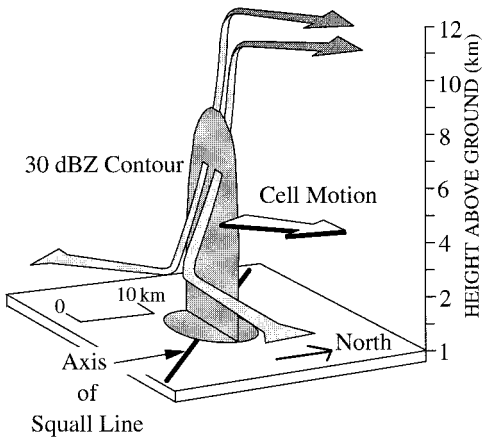

FIG. 7. Schematic of the airflow (shaded 3D arrows) relative to the motion of a cell comprising the squall line. The white arrow shows the direction toward which the cell moved. The long axis of the squall line is shown by the heavy solid line.

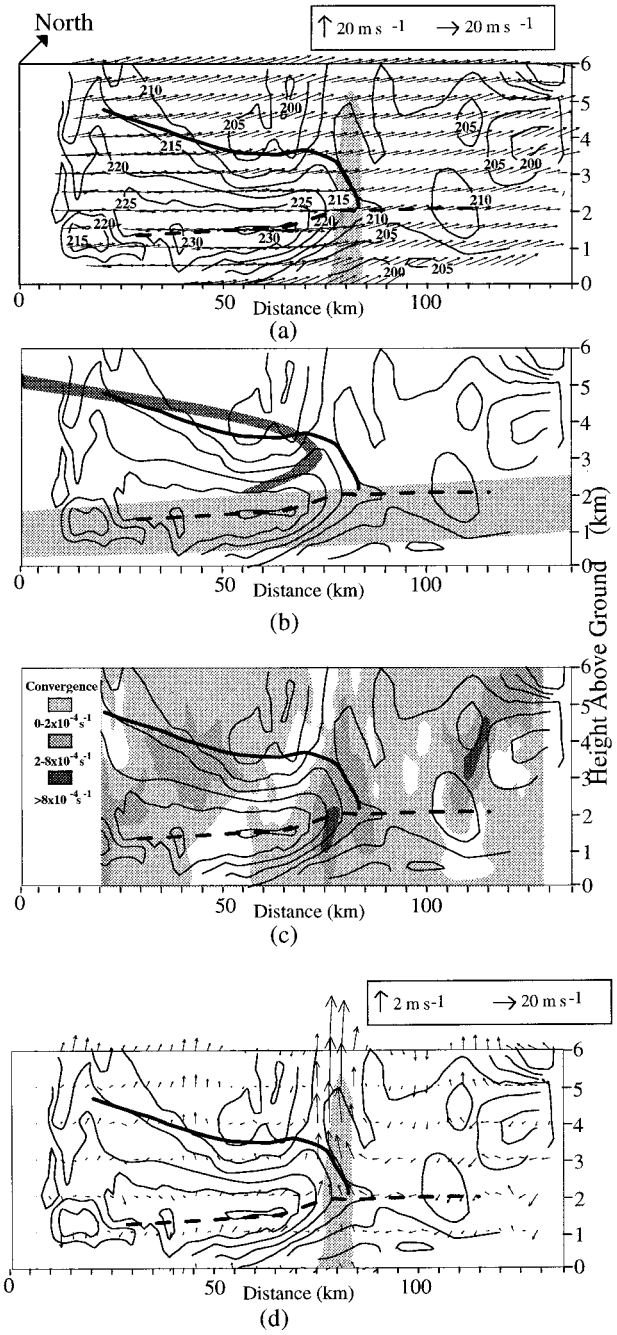

FIG. 8. (a) Contours of the direction from which the horizontal wind was blowing (labeled in degrees compass direction) and vectors of the horizontal winds in a vertical cross section along the x axis from $x = 0$ to $x = 135$ km averaged from $y = 0$ to $y = 105$ km. Radar reflectivities greater than 30 dBZ are shown by shading. (b) As for (a) but showing the interpolated position of the tongue of high-θ_e air from Fig. 3 (light shading), the interpolated position of the CFA from Fig. 3 (dark shading), the leading edge of the region of cold advection (heavy solid line), and the top of the region of warm advection (heavy dashed line). (c) As for (a) but showing convergence. (d) As for (a) but showing storm relative wind vectors in the cross section.

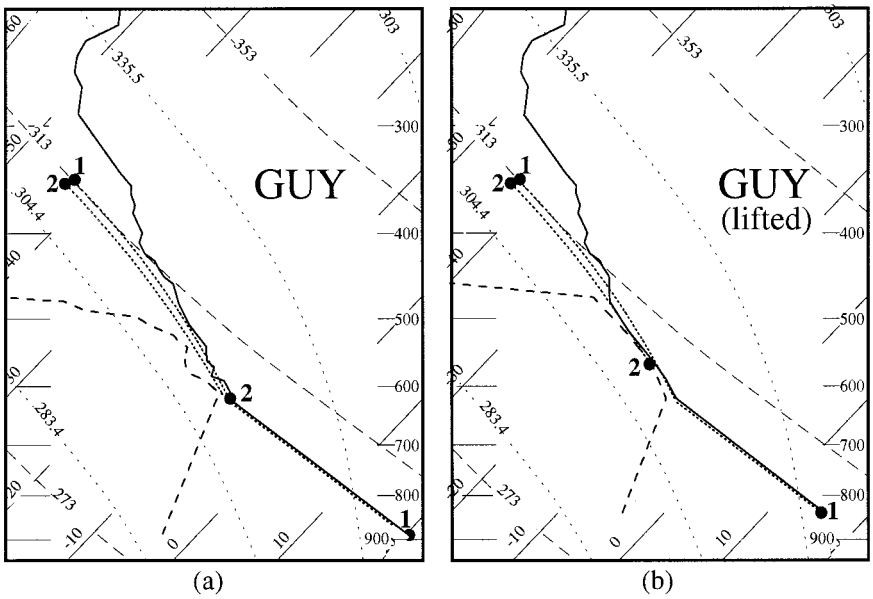

FIG. 9. (a) Sounding of temperature (heavy solid line) and dewpoint (heavy dashed line) from Guymon, Oklahoma (GUY) at 2305 UTC 8 March 1992. The slanted short light lines are isotherms (°C). The light dashed lines are dry adiabats (K). The light dotted lines are wet adiabats (K). The heavy dotted lines and numbered circles show the lifted paths for selected air parcels (labeled 1 and 2). (b) As for (a), but with the sounding in (a) undergoing column lifting. See text for further explanation.

data are available for this stage of the squall line discussed here. Thus, the external lifting mechanism that initiated or helped to maintain this squall line cannot be quantified. Therefore, the following stability analysis is carried out with the goal of determining *how much* lifting was required to bring low-level parcels to their LFC.

First, the environmental stability is examined immediately prior to the initiation of the squall line. The first identifiable radar echo associated with the squall line is the line echo 40 km west of Guymon at 0000 UTC 9 March (Fig. 2a). From Figs. 3a and 3b, it is known that the squall line developed approximately at the time that the CFA moved over the drytrough. The most relevant rawinsondes prior to the initiation of the squall line were launched from GUY (Fig. 9a) and DDC (Fig. 10a) shortly after 2300 UTC 8 March. The cross-sectional analysis in Fig. 3a shows that at 2300 UTC 8 March GUY was located west of the drytrough but east of the CFA, whereas DDC was located east of both the drytrough and CFA. The GUY and DDC soundings were launched approximately 1.5 and 2.5 h before the passage of the squall line at their respective locations. For each sounding, selected air parcels were lifted to find their LFC; the lifting was then continued at the moist-adiabatic rate to obtain their convective available potential energy (CAPE). However, if it is assumed that some form of organized mesoscale ascent caused the initiation of the squall line, it is more appropriate to examine the soundings in terms of column lifting (i.e., convective or potential instability), rather than parcel lifting (i.e., conditional instability). Therefore, for each sounding, a layer from the surface to 550 hPa was lifted by 50 hPa, with the amount of lifting decreasing linearly to 0 hPa between 550 and 450 hPa. The lifted soundings are shown in Figs. 9b and 10b. The amount of layer lifting used (50 hPa) represents a zone of moderate mesoscale convergence (10^{-4} s^{-1}), integrated through a depth of 1 km to produce a vertical velocity of 10 cm s^{-1}, acting on a parcel for a period of 1–2 h. As was done for the two unlifted soundings, selected parcel ascents are shown to demonstrate their stability.

Without any column lifting, representative air parcels from the GUY sounding never reach the LFC (Fig. 9a). After column lifting of 50 hPa, air parcel 2 from the top of the well-mixed layer is never buoyant, and air parcel 1 still needs 220 hPa of lift to reach its LFC, after which it is only weakly buoyant for a depth of 100 hPa (Fig. 9b). In contrast, the air in the DDC sounding is more unstable. In the unlifted sounding (Fig. 10a), air parcels 1 and 2 become temporarily buoyant with 60 and 160 hPa of lift, respectively, but both parcels require an additional 140 hPa ascent to break through the capping inversion at 650 hPa. Air parcel 3 requires 180 hPa of lift to reach its LFC. However, with 50 hPa of column lifting (Fig. 10b), parcel 1 requires only 90 hPa of additional lift through a well-mixed layer to reach its LFC, and parcels 2 and 3 are immediately buoyant. The buoyant energy of the parcels increases when the DDC sounding undergoes column lifting.

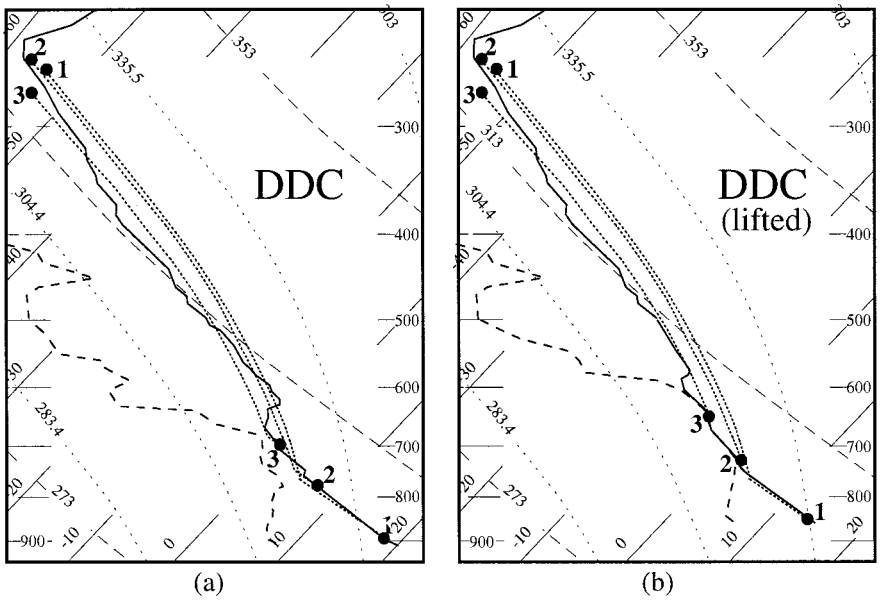

FIG. 10. As for Fig. 9 but for Dodge City, Kansas (DDC), for 2329 UTC 8 March 1992.

These soundings are representative of the conditions of the atmosphere on either side of the drytrough, and indicate the potential for convection in those regions before and after the arrival of the CFA. Therefore, one might expect that prior to the arrival of the CFA (as represented by the unlifted soundings), there would have been no convection west of the drytrough, with, perhaps, scattered convection east of the drytrough. After the arrival of the CFA, and its attendant mesoscale lifting (as represented by the lifted soundings), the area west of the drytrough might have supported weak convection, but the area east of the drytrough would have been characterized by significant convection organized according to the pattern of the mesoscale ascent. These predictions are consistent with Figs. 2a and 2b.

The above discussion addresses the issue of squall line initiation. However, it is also important to consider the requirements for squall line maintenance. We would like to answer the question, how much lifting is required to bring parcels immediately ahead of the mature squall line to their LFC? To address this question, we will examine the sounding from TOP at 0511 UTC 9 March 1992. This sounding was taken about 2 h prior to the time the squall line passed through the area scanned by the dual-Doppler radars. As was done for the GUY and DDC soundings, the TOP sounding is shown in two panels. The first panel shows the results of lifting selected air parcels with no column lifting, and the second panel shows the result of lifting the same air parcels after the sounding has undergone column lifting similar to that for the DDC sounding.

Comparing Figs. 11a and 11b, it can be seen that an air parcel near the surface and below the tongue of high-θ_e air (parcel 1) never becomes buoyant when lifted, even when the sounding is modified by column lifting. Air parcels 2 and 3, within the tongue of high-θ_e air, need about 110–150 hPa of lift to become buoyant with no column lifting, but they are immediately buoyant to the tropopause with column lifting. In contrast, air parcel 4, which is just above the tongue of high-θ_e air, needs 60 hPa of lifting in addition to the column lifting, to become slightly buoyant, and significant buoyancy is achieved only up to 500 hPa. It is also evident that for parcels 2 and 3 column lifting increases the CAPE in the midtropospheric portion of the ascent. The lack of buoyancy of the near-surface air parcel 1, and the buoyancy of the more elevated parcels 2 and 3, is consistent with the maximum inflow (Fig. 5) and convergence (Fig. 8d) being elevated from 1 to 4 km above the surface.

As mentioned previously, it is not possible to quantify how much of the initial ascent in the mature squall line is due to the squall line itself (through its buoyancy-driven circulation and through the forced lifting from its cold pool) and how much is due to external mesoscale lifting. However, the analysis of the TOP sounding suggests that while a moderate parcel ascent of 1–2 km, which might have been provided by the squall line itself, would have been sufficient to maintain the squall line, a smaller amount of column lifting (~0.5 km), which could have been provided by the mesoscale ascent associated with the CFA, would have released convective instability and increased the CAPE for parcel ascent.

5. Comparisons with theory and previous case studies of midlatitude squall lines

It is of interest to compare the midlatitude squall line discussed here with other squall lines that have been studied and numerically modeled. The squall line that occurred on 10–11 June 1985 in Kansas and Oklahoma,

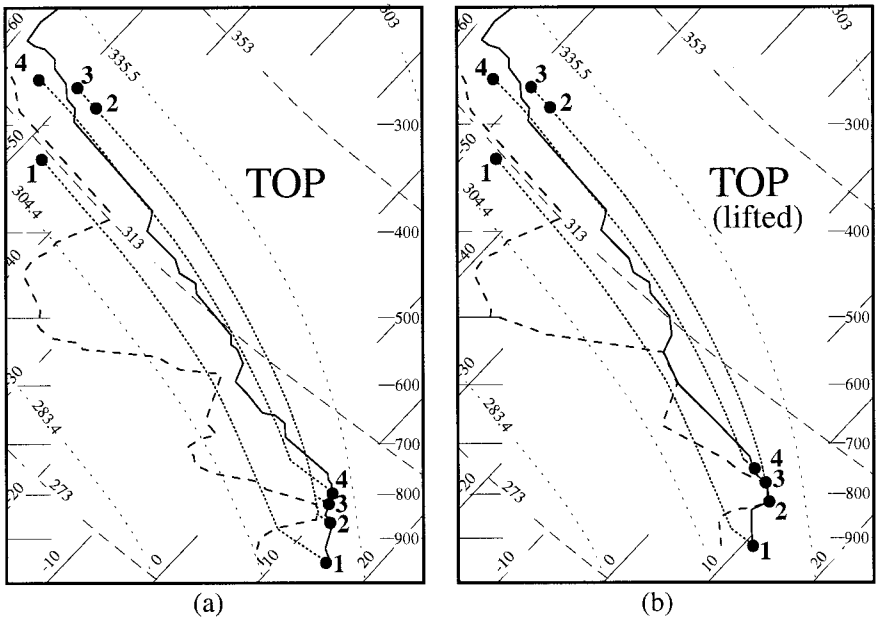

FIG. 11. As for Fig. 9 but for Topeka, Kansas (TOP), at 0511 UTC 9 March 1992.

as reported by Biggerstaff and Houze (1993) and Braun and Houze (1994), is used as an initial basis of comparison. That squall line is an archetypical example of the Houze et al. (1989) ''leading line/trailing stratiform'' (LL/TS) conceptual model for midlatitude squall lines. Although the LL/TS model is by no means the only type of midlatitude squall line that has been observed, it represents a large class of ''ordinary'' cell (nonsupercell) squall lines that have been produced under a range of vertical shear conditions in numerical models (e.g., Weisman et al. 1988; Fovell and Ogura 1989). Also, the LL/TS type of squall line has been observed in both intensive case studies [e.g., the 22 May 1976 case (Smull and Houze 1985) and the 10–11 June 1985 case (Biggerstaff and Houze 1993)], and in MCS climatologies (e.g., Houze et al. 1990). However, several noteworthy squall lines have not conformed to the LL/TS model; many of those that do not display supercellular characteristics (e.g., Newton 1966; Fankhauser et al. 1992).

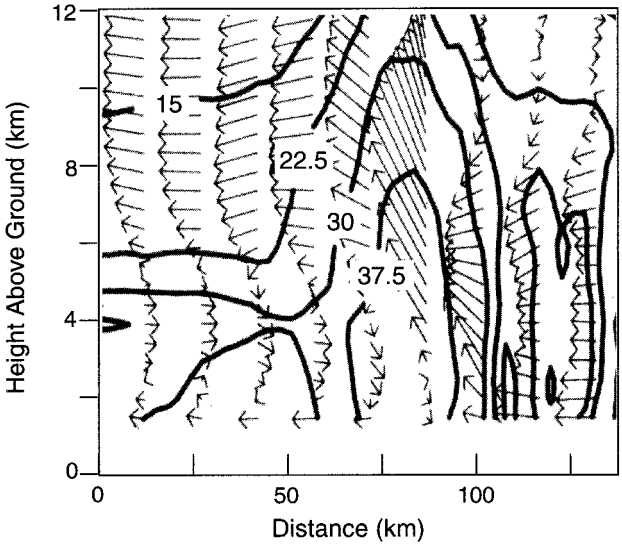

FIG. 12. A portion of Fig. 1a from Braun and Houze (1994) for a squall line over Kansas and Oklahoma on 10–11 June 1985, showing a cross section of radar reflectivity (contoured every 7.5 dBZ) averaged over the length of the squall line and storm-relative wind vectors in the plane of the cross section (vector scale shown in upper right). For the purpose of comparison, the original figure has been cropped to exactly match the horizontal and vertical extent of Fig. 5 of the present paper.

To facilitate a comparison between the present case and the 10–11 June 1985 case, a dual-Doppler-derived cross section through that squall line, adapted from Braun and Houze (1994), has been enlarged and cropped so that the distance and height ranges are identical to those in Fig. 5. This cross section is shown in Fig. 12. Several differences are evident between the two squall lines. First, the 10–11 June squall line had a rearward sloping updraft, whereas, the 8–9 March squall line had essentially a vertical updraft. Second, in the 10–11 June case, the divergent outflow above the main updraft exited primarily to the rear of the squall line in a deep, weakly ascending layer above 5 km. In the 8–9 March case, the outflow was exclusively forward, with no ascending front-to-rear flow aloft behind the squall line. Third, the 10–11 June squall line had a definite trailing stratiform rain region (as evidenced by the bright band at 3.5-km height between $x = 0$ and $x = 50$ km), whereas, the 8–9 March squall line was characterized by intermittent weaker convective cells behind the main convective line. Fourth, the 10–11 June squall line had a

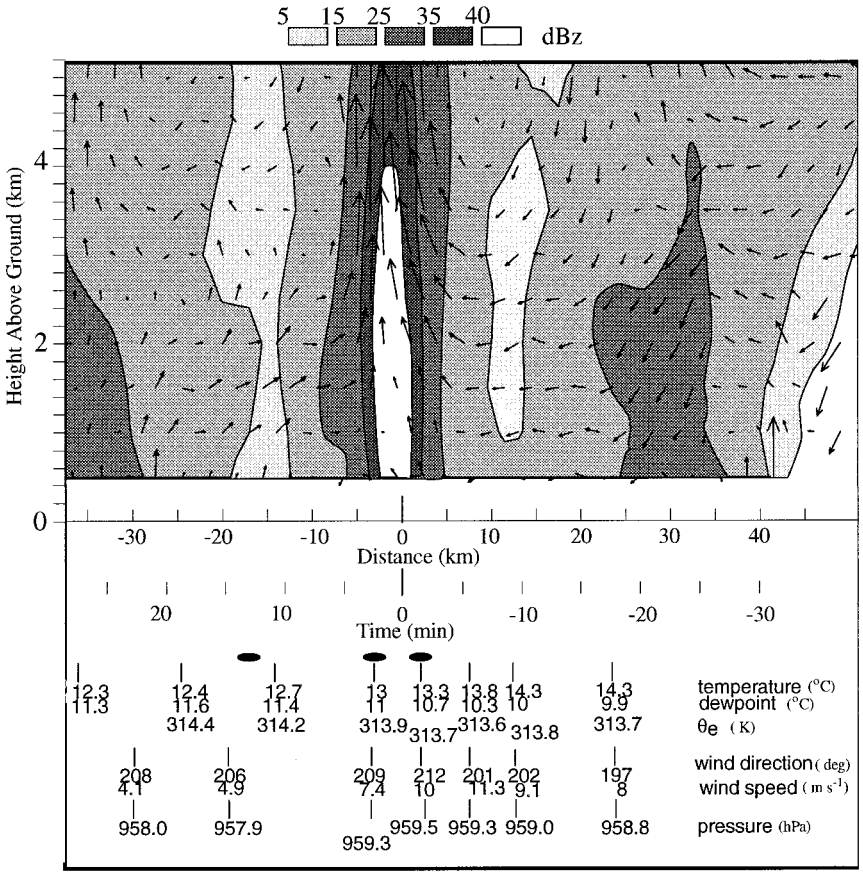

FIG. 13. An enlarged view of a portion of Fig. 5, in the immediate low-level vicinity of the main convective line (from $x = 42$ to $x = 130$ km), showing the storm-relative wind vectors and radar reflectivity. Underneath the plot are time series of temperature (°C), dewpoint (°C), θ_e (K), wind direction (°), wind speed (m s^{-1}), and pressure (hPa) from the Havensville, Kansas, PAM surface station; the data have been time-to-space transformed to correspond to the position of the squall line. The black ellipses indicate times when precipitation was recorded.

rear-to-front flow, which was approximately coincident with the radar bright band and moved forward and downward toward the leading edge of the squall line; the 8–9 March squall line had no well-defined rear inflow. Fifth, the rear and lower portions of the high radar reflectivity column in the 10–11 June squall line were characterized by a well-defined downdraft and a low-level outflow (i.e., a cold pool), the top of which can be seen clearly near $x = 90$ km and $z = 2$ km. On the other hand, as mentioned previously, the 8–9 March squall line showed no evidence of a cold outflow above 1 km, and the downdrafts were intermingled with the updrafts in the along-line direction (see Fig. 6), so they do not appear in the averaged cross section. A final interesting difference, which is not evident from the cross sections, is that the time evolution suggested by the LL/TS model involves cells that move backward relative to the line as they initiate, grow, and decay, such that the ground-relative cell speed normal to the line is typically less than the overall squall line speed. However, in the 8–9 March squall line, the cell motion normal to the squall line is nearly identical with the overall squall-line speed, indicating that the cell position is steady relative to the squall line. This fact does not necessarily indicate that the cells themselves are long-lived. The question of whether or not the squall line consisted of long-lived supercells is addressed below.

The cold pool in the 8–9 March case is of particular interest, and merits further analysis. Generally speaking, a cold pool that is formed by evaporatively cooled downdrafts is recognized as a key structural feature of squall lines, because it provides the initial lifting necessary to bring incoming low-level air to its LFC. This is certainly true in the LL/TS conceptual model. A review of observed and simulated midlatitude squall lines shows that cold pool temperature deficits range from 4° to 10°C, with an associated surface pressure jump of 2–3 hPa. The dual-Doppler and surface observational data show that in the present squall line, the cold pool was comparatively weak. Figure 13 shows an enlarged view of the lower portion of the squall line from Fig. 5. Because of the lack of dual-Doppler data at the lowest

levels, it is difficult to develop a clear picture of the structure, depth, and position of the cold pool. The storm-relative flow signature that one would expect to see with a cold pool is weak horizontal motion and zero or downward vertical motion. However, Fig. 13 shows that the winds at 1.5 km are rising or flowing strongly into the updraft, and are not consistent with those within a cold pool; thus, the cold pool did not appear to exceed 1.5 km in depth. Time series of various meteorological quantities are shown in Fig. 13. These time series are from the Havensville PAM station (see Fig. 1 for its location relative to dual-Doppler domain), and have been time-to-space transformed to the cross section using the observed squall line speed and equating the time of maximum precipitation at Havensville to the maximum near-surface reflectivity in the cross section. The right-most pressure shown in Fig. 13 represents that of the quiescent pre-squall-line environment. Approximately 10 km ahead of (or 8 min before) the leading edge of high reflectivity, the temperature begins to decrease and pressure begins to increase, signaling the arrival of the cold pool. The 10-km offset between the leading edge of the cold pool and the onset of heavy precipitation is consistent with that seen in other studies (e.g., Heymsfield and Schotz 1985; Johnson and Hamilton 1988). From the leading edge of the cold pool to the passage of the high precipitation core, the temperature drops only 1.3°C, and the pressure rises only 0.5 hPa.

Four other PAM time series in the vicinity were examined. The average cold pool temperature and pressure perturbations for the five stations were 1.3°C and 1.2 hPa, respectively. Earlier in the squall line's life cycle, PAM stations and surface synoptic stations in central and eastern Kansas showed pressure jumps of anywhere from less than 1 to 4 hPa, and temperature drops of 1°–4°C. The largest values occurred at around 0500 UTC 9 March, approximately 4 h after squall-line initiation. Although the cold pool had apparently diminished in strength between that time and the dual-Doppler analysis time (0740 UTC 9 March), the storm was still mature in terms of the vigor of its updrafts and the intensity of its radar echoes, and strong echoes could be followed in the radar summary for 5 h beyond the time of the analysis.

In summary, at the time of the dual-Doppler analysis presented here, the squall line we have discussed in this paper differed from the LL/TS conceptual model in virtually every significant aspect. We will now discuss these differences in terms of environmental factors that are known to effect the structure and dynamics of squall lines.

Recent research on midlatitude squall lines has emphasized the effect of the environmental wind shear profile on squall-line strength, structure, and evolution. Studies by Thorpe et al. (1982), Rotunno et al. (1988), and Weisman et al. (1988), have demonstrated that the strength of a squall line is optimized when the shear at low levels (through a depth equal to that of the cold pool) is close to an optimum value. Rotunno et al. (1988) established this optimum value of low-level shear as that which exactly balances the baroclinic generation of vorticity by the cold pool. In this optimum case, the low-level environmental inflow is forced into an upright jet that quickly brings near-surface air to its LFC. However, except in the case of very large low-level shear, nonsupercell squall lines that have been modeled (e.g., Weisman et al. 1988; Fovell and Ogura 1989) typically evolve from a greater-than-optimal shear state to a suboptimal shear state as they develop increasingly stronger cold pools, and can achieve a steady state in suboptimal low-level shear (Fovell and Ogura 1989). In addition to low-level shear, deeper shear can dramatically effect squall-line structure. The three-dimensional modeling study by Weisman et al. (1988) showed that the presence of deeper environmental shear (into the midtroposphere) can transform what is otherwise an essentially two-dimensional system into a more complex three-dimensional structure with rotating updrafts and significant flow between cells. In extreme cases, deeper shear can result in a squall line that is essentially a line of supercell thunderstorms. Finally, strong upper-tropospheric shear can be a determining factor in the direction of the squall-line anvil outflow.

Numerical modeling studies have focused almost exclusively on shear at lower or middle levels, typically using constant shear in the upper troposphere, and thus have produced either rearward-only (i.e., upshear) or split forward and rearward anvil outflows [an exception to this is the strongest deepest shear case in (Weisman et al. 1988)]. Cases described in the literature also tend to have weak shear in the upper troposphere, producing either forward or split anvil outflows. However, Fankhauser et al. (1992) examined a Montana squall line in which the environment was characterized by a pronounced line-normal jet at 10 km that resulted in a forward-only anvil outflow. Such an anvil outflow precludes the formation of the trailing stratiform region, a feature that has been seen in several studies of midlatitude squall lines (i.e., the LL/TS model).

The environmental line-normal wind profile for the present case, obtained from two different sources, is shown in Fig. 14. The first profile was obtained by averaging all the available dual-Doppler winds to the right of the line defined by $x = 90$ km in Fig. 4. Reliable data were not available below 1 km because of the slight elevation angle of the lowest radar scan, and because of the curvature of the earth. In place of that data, the storm-relative surface wind at 0715 UTC 9 March at the Havensville, Kansas, PAM station (15 min prior to the passage of the squall line—see Fig. 1 for location of Havensville PAM station) is shown as a dashed arrow in Fig. 14 to give some indication of the lowest portion of the profile. It should be noted that even though the primary convective line was excluded from the average, the fact that radar echoes were present in the averaging

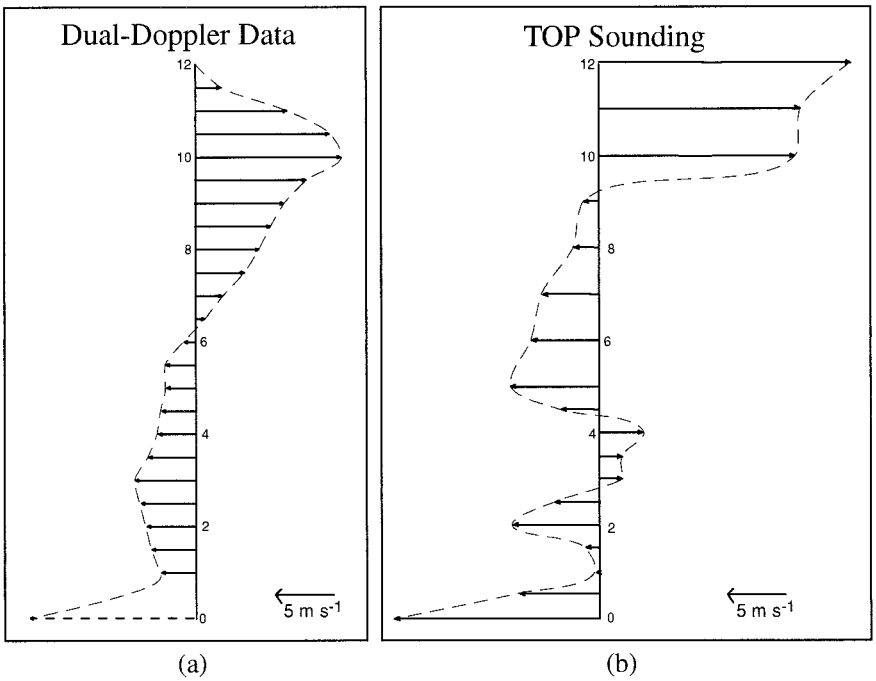

FIG. 14. Vertical profiles of the wind components perpendicular to the axis of the squall line and relative to its motion. (a) Winds averaged from the dual-Doppler data in the pre-squall-line environment at 0740 UTC 9 March 1992. Data is unreliable below 1 km, but a surface wind from a nearby PAM surface station (Havensville, Kansas) just prior to the arrival of the squall line has been added to complete the profile. (b) Winds from the sounding launched from Topeka, Kansas (TOP), at 0511 UTC 9 March 1992.

area implies that this volume of air was already affected by the weaker convective precipitation ahead of the primary line. As a further illustration of the wind profile ahead of the squall line, the environmental wind component perpendicular and relative to the squall line from the TOP sounding (elevation 269 m) launched at 0511 UTC 9 March (2.5 h prior to squall-line passage) is shown on the right of Fig. 14.

Both profiles generally show strong shear in the lowest 1 km, followed by weak or variable shear in the layer from 1 to 6 km. In the upper troposphere, shear increases again, culminating in a strong line-normal jet at 10–12 km, likely contributing to the fact that the anvil outflow was primarily in the forward (downshear) direction, as was discussed above. The wind profile from Hillsboro in east-central Kansas (not shown), which the squall line passed at around 0530 UTC (2 h before its passage at the dual-Doppler site), showed a similar shear structure.

Since the squall line described in this paper produced damaging hail and an F0 tornado, we will now examine the possibility that it consisted of long-lived supercells. Weisman et al. (1988) showed that strong, *deep* shear is conducive to cell splitting, rotating updrafts, and supercellular structure, and they pointed out that several squall lines reported in the literature were actually lines of quasi-steady supercells. Although this special type of squall line typically has a strong cold pool, the lack of that feature in the present case does not preclude the possibility of supercellular structure, because supercells also force vertical motion through a dynamically induced vertical pressure gradient (Rotunno and Klemp 1982).

In the present case, the pre-squall-line environment had moderate shear up to 1.5 km (around 10–15 m s^{-1}), but weak or variable shear from 1.5 to 6 km (Fig. 14). While it is possible for strong shallow shear alone to cause storm splitting and rotating updrafts [e.g., Weisman et al. (1988) produced such a storm with 25 m s^{-1} shear in the lowest 2.5 km], the shear in this case clearly does not seem strong enough or deep enough to be conducive to supercell formation. The signature of supercells in a squall line is the presence of rotating updrafts, which can be elucidated by examining the correlation between vorticity and vertical velocity in the midtroposphere. The correlation coefficient r was calculated from the dual-Doppler-derived wind fields, and found to be less than or equal to 0.1 at all levels, indicating a lack of consistently rotating updrafts.

A second signature of supercellular squall lines is the persistence of steady cells, as opposed to continually growing and decaying cells. Unfortunately, the data in this case were not frequent enough, and did not cover a sufficient period of time, to ascertain the steadiness of cells. However, the available evidence mentioned above are sufficient to conclude that the squall line most

likely did not consist of supercell structure at the time of our dual-Doppler analysis. At earlier times, we have no dual-Doppler data to elucidate cell type. However, as mentioned above, the Hillsboro, Kansas, wind profiler (which the squall line passed 2 h prior to the dual-Doppler analysis time) showed a similar shear profile to that at the analysis time, suggesting that the environment was also not conducive to supercell formation at that time either.

The magnitude of the low-level wind shear shown in Fig. 14 and the cold pool information described above, can be used to assess the optimality of the cold pool/wind shear balance in this case. Rotunno et al. (1988) define the relevant low-level shear as the change in the wind component perpendicular to the squall line (Δu) through a depth equal to the height of the cold pool. The vorticity balance analysis of Rotunno et al. showed that the optimal shear is such that Δu is equal to the speed with which the cold pool would travel through a fluid at rest that has the same thermal profile as the environment ahead of the squall line. This speed (V) is typically calculated from the height and virtual temperature perturbation of the cold pool:

$$V = \left(2gh\frac{T_{v1} - T_{v2}}{T_{v2}}\right)^{1/2},$$

where, g is acceleration due to gravity, h the height of the cold pool, and T_{v1} and T_{v2} are the average virtual temperatures in the warm and cold air, respectively. In the present case, the height of the cold pool is not known, but can be estimated to have a value of, at most, 1.5 km, based on the velocity structure seen in Fig. 13. The vertical variation of the temperature perturbation through the depth of the cold pool must also be assumed. For lack of better information, we assume a linear decrease in perturbation temperature through the depth of the cold pool, roughly consistent with cold pool thermal structures shown in the simulated squall lines of Weisman et al. (1988). The contribution to the temperature perturbation from virtual temperature effects was found to be much less than 1°C and is neglected. Using the five-station average temperature perturbation reported above, a cold pool speed of 8 m s^{-1} was obtained.

Another method for calculating the speed of the cold pool is to use Seitter and Muench's (1985) formula, which uses the pressure perturbation instead of the temperature perturbation

$$V = \left(\frac{\Delta p}{\rho}\right)^{1/2},$$

where Δp is the surface pressure perturbation associated with the density current and ρ is the density of the warm air. The advantage of this method is that it does not require assumptions about cold pool depth and vertical thermal structure. However, it does not strictly conform to the Rotunno et al. (1988) theory because, although it expresses the correct cold pool speed in a still environment, it includes pressure effects from above the cold pool that are not included in the vorticity balance analysis of Rotunno et al. (1988). Therefore, it is used here only as a check on the reasonableness of the temperature method. Using the five-station average pressure perturbation of 1.2 hPa, the pressure method yields a speed of 10 m s^{-1}, roughly consistent with the temperature method. In comparison, the average Δu through 1.5 km for the two wind profiles shown in Fig. 14 is 14 m s^{-1}. Thus, at the time of the dual-Doppler analysis, this convective system can be described as a mature squall line that is persisting in a greater-than-optimal shear environment. This condition is inconsistent with most of the numerically simulated non-supercell squall lines described by Weisman et al. (1988) and Fovell and Ogura (1989), which show, for a wide range of low-level shear values, that the predominant evolution is from an initially greater-than-optimal to a long-lived suboptimal shear state. Rotunno et al. (1988) found that in a 2D simulation of a squall line in greater-than-optimal shear, the forward-leaning updrafts drop precipitation into the low-level inflow, cooling and slowing the squall line. However, we have already shown that in the present case, even though the updrafts are vertical in the cross-line direction, their tilt in the along-line direction allows for the precipitation to fall primarily between the updrafts. Therefore, even though the squall line did not appear to display supercell characteristics, the three-dimensional structure of the line was still important in this case.

If it is assumed that the present squall line was driven by convergence at the cold pool, it might be concluded that it occupies a unique and interesting position in the shear/cold pool parameter space for mature, ordinary cell squall lines. However, our interpretation is different. Based on the thermodynamic profile of the pre-squall-line environment, and the height of the inflow feeding the updraft, it may well be the case that the strength of the cold pool and its ability to force surface air into an upright updraft was not relevant for the maintenance of this squall line. As already mentioned, air below 1 km in the pre-squall-line environment was not buoyant (see the 0511 UTC 9 March Topeka, Fig. 11a), and the air velocity and convergence fields derived from dual-Doppler data (Figs. 5 and 8c) show that inflow and convergence were maximized between 1 and 4 km. The stable boundary layer in this case makes it somewhat unique among squall lines that have been observed and modeled, most of which start out with CAPE maximized for surface air parcels. However, it is not necessarily uncommon among all midlatitude mesoscale convective systems (MCS). Houze et al. (1990), in a climatological study of MCS in Oklahoma, found that MCS often develop in environments with low-level stability, although the convective activity tends to be ''unfocused.'' They attributed this ''unfocused'' characteristic to the fact that ''moist, stable low-level conditions (such as those frequently observed on the cool side of a stationary or

warm-frontal boundary) would act to impede the establishment of penetrative downdrafts driven by evaporation and negative buoyancy.'' It should be noted that the environment through which the 9 March 1992 squall line propagated was on the cool side of a drytrough, a feature that Hobbs et al. (1996) describe as similar to a warm front. Houze et al. (1990) go on to say that in the absence of penetrative downdrafts, ''development of a mesoscale cold pool (and the accompanying arc-like mesoscale band of convergence along its expanding boundary) might be retarded or prevented altogether.'' In the present case, however, focused linear organization of the convective system was maintained in spite of the environment not being conducive to cold pool formation, which suggests the possibility that another focusing mechanism, such as the coincident CFA, was involved. This explanation gains merit when the squall line is viewed in the larger, synoptic-scale context (Fig. 1), which shows that a series of squall lines extended in a nearly 2000-km-long arc that closely matched the position of the CFA (Locatelli et al. 1995).

6. Conclusions

On 8–9 March 1992, a long-lived squall line traversed the state of Kansas and produced hail and damaging winds. In an earlier study (Locatelli et al. 1995) we showed that this squall line was part of a synoptic-scale rainband that was associated with a cold front aloft (CFA), a feature that is a key component of the STORM conceptual model for cyclones in the central United States (Hobbs et al. 1996). In this paper, we have examined in detail the mesoscale structure of this squall line and its relationship to the CFA.

Analysis of synoptic-scale cross sections, based on rawinsonde ascents, shows that the squall line was likely associated with the CFA. A more detailed mesoscale cross section of winds, derived from dual-Doppler radar data, shows that the squall line was exactly coincident with the ''nose'' of the CFA. The dual-Doppler analysis shows that the inflow to the squall line was elevated, drawing in air from a potentially unstable layer within a weak warm frontal–like feature that was being occluded by the CFA. Stability analysis of soundings near the location where the squall line formed, as well as in the environment ahead of the mature squall line, shows that once the CFA overtook the surface position of the drytrough, the thermal and moisture structure of the atmosphere was such that a moderate amount of column lifting, which could have been provided by an organized mesoscale ascent, could have released convective instability within an elevated layer (~1–2 km AGL) that would have rendered parcels buoyant to the tropopause.

A comparison was made between the structure of this squall line and the ''leading line/trailing stratiform'' conceptual model described by Houze et al. (1989). The mesoscale structure of the squall line described in this paper differs substantially from that conceptual model in virtually every significant aspect. These differences included the absences of: a strong cold pool, a front-to-rear outflow aloft behind the squall line, a rear-to-front inflow behind the squall line at mid-levels, and a region of stratiform rain; but, the presence of a forward outflow aloft.

The possibility that this squall line was a line of steady supercells was investigated. We found that the deep shear profile was not conducive to supercell formation, and no evidence of rotating updrafts could be found in the dual-Doppler velocity data. Thus, at the time of our dual-Doppler analysis (7 h into its life cycle), it is more likely that the squall line was comprised of ordinary growing and decaying cells, rather than supercells. Finally, we examined the balance between the strength of the cold pool and the low-level shear, which, according to the theory of Rotunno et al. (1988), is important for the maintenance of a strong, upright convective line. Unlike many observed and modeled squall lines, which tend to evolve from an early stage in greater-than-optimal shear to a mature stage in suboptimal shear, the present squall line was found to be in a greater-than-optimal shear state at around 7 h into its lifetime, when it was near the middle or later part of its mature stage. However, the balance between low-level shear and cold pool strength may have been of secondary importance, because the environment through which the squall line propagated was characterized by an elevated layer of instability overlying a stable boundary layer. The weakness of the surface cold pool, and the elevated inflow and convergence associated with the convection, suggest that the focusing mechanism for the squall line was also elevated.

With regard to understanding the mechanism that organized this squall line, these facts shift attention away from the surface cold pool and toward the CFA, the leading edge of which was coincident with the squall line. The suggestion that the lifting associated with the CFA acted as a focusing mechanism for the squall line is supported by the fact that, when viewed on the synoptic scale (Fig. 1), the squall line described here is seen to be one of a series of squall lines that extended in a nearly 2000-km-long arc that closely matched the position of the CFA.

Acknowledgments. This research was supported by Grant ATM-9632580 from NSF's Division of Atmospheric Sciences, Mesoscale Dynamic Meteorology Program.

REFERENCES

Biggerstaff, M. I., and R. A. Houze Jr., 1993: Kinematics and microphysics of the transition zone of the 10–11 June 1985 squall line. *J. Atmos. Sci.,* **50,** 3091–3110.

Braun, S. A., and R. A. Houze Jr., 1994: The transition zone and secondary maximum of radar reflectivity behind a midlatitude squall line: Results retrieved from Doppler radar data. *J. Atmos. Sci.,* **51,** 2733–2755.

Castle, J. A., J. D. Locatelli, J. E. Martin, and P. V. Hobbs, 1996: Structure and evolution of winter cyclones in the central United States and their effects on the distribution of precipitation. Part IV: The evolution of a drytrough on 8–9 March 1992. *Mon. Wea. Rev.,* **124,** 1591–1595.

Eliassen, A., 1962: On the vertical circulation in frontal zones. *Geofys. Publ.,* **24,** 147–160.

Emanuel, K. A., 1985: Frontal circulations in the presence of small moist symmetric stability. *J. Atmos. Sci.,* **42,** 1062–1071.

Fankhauser, J. C., G. M. Barnes, and M. A. LeMone, 1992: Structure of a midlatitude squall line formed in strong unidirectional shear. *Mon. Wea. Rev.,* **120,** 237–260.

Fovell, R. G., and Y. Ogura, 1989: Effect of vertical shear on numerically simulated multicell storm structure. *J. Atmos. Sci.,* **46,** 3144–3176.

Fujita, T. T., 1981: Tornadoes and downbursts in the context of generalized planetary scales. *J. Atmos. Sci.,* **38,** 1511–1534.

Heymsfield, G. M., and S. Schotz, 1985: Structure and evolution of a severe squall line over Oklahoma. *Mon. Wea. Rev.,* **113,** 1563–1589.

Hobbs, P. V., J. D. Locatelli, and J. E. Martin, 1996: A new conceptual model for cyclones generated in the lee of the Rocky Mountains. *Bull. Amer. Meteor. Soc.,* **77,** 1169–1178.

Houze, R. A., Jr., S. A. Rutledge, M. I. Biggerstaff, and B. F. Smull, 1989: Interpretation of Doppler weather radar displays of midlatitude mesoscale convective systems. *Bull. Amer. Meteor. Soc.,* **70,** 608–619.

——, B. F. Smull, and P. Dodge, 1990: Mesoscale organization of springtime rainstorms in Oklahoma. *Mon. Wea. Rev.,* **118,** 613–654.

Johnson, R. H., and P. J. Hamilton, 1988: The relationship of surface pressure features to the precipitation and airflow structure of an intense midlatitude squall line. *Mon. Wea. Rev.,* **116,** 1444–1472.

Locatelli, J. D., J. E. Martin, J. A. Castle, and P. V. Hobbs, 1995: Structure and evolution of winter cyclones in the central United States and their effects on the distribution of precipitation. Part III: The development of a squall line associated with weak cold-frontogenesis aloft. *Mon. Wea. Rev.,* **123,** 2641–2662.

——, M. T. Stoelinga, R. D. Schwartz, and P. V. Hobbs, 1997: Surface convergence induced by cold fronts aloft and prefrontal surges. *Mon. Wea. Rev.,* **125,** 2808–2820.

Martin, J. E., J. D. Locatelli, P. V. Hobbs, P.-Y. Wang, and J. A. Castle, 1995: Structure and evolution of winter cyclones in the Central United States and their effects on the distribution of precipitation. Part I: A synoptic-scale rainband associated with a dryline and lee trough. *Mon. Wea. Rev.,* **123,** 241–264.

Mohr, C. G., and C. J. Miller, 1983: CEDRIC—A software package for Cartesian space editing, synthesis, and display of radar fields under interactive control. Preprints, *21st Conf. on Radar Meteorology,* Edmonton, AB, Canada, Amer. Meteor. Soc., 559–574.

——, ——, and R. L. Vaughn, 1979: An economical procedure for Cartesian interpolation and display of reflectivity factor data in three-dimensional space. *J. Appl. Meteor.,* **18,** 661–670.

Newton, C. A., 1966: Circulations in large sheared cumulonimbus. *Tellus,* **18,** 699–713.

Oye, R., and R. E. Carbone, 1981: Interactive Doppler editing software. Preprints, *20th Conf. on Radar Meteorology,* Boston, MA, Amer. Meteor. Soc., 683–689.

Rotunno, R. J., and J. B. Klemp, 1982: The influence of the shear-induced pressure gradient on thunderstorm motion. *Mon. Wea. Rev.,* **110,** 136–151.

——, ——, and M. L. Weisman, 1988: A theory for strong, long-lived squall lines. *J. Atmos. Sci.,* **45,** 463–485.

Sawyer, J. S., 1956: The vertical circulation at meteorological fronts and its relations to frontogenesis. *Proc. Roy. Soc. London,* **A234,** 346–362.

Seitter, K. L., and H. S. Muench, 1985: Observation of a cold front with rope cloud. *Mon. Wea. Rev.,* **113,** 840–848.

Smull, B. F., and R. A. Houze, 1985: A midlatitude squall line with a trailing region of stratiform rain: Radar and satellite observations. *Mon. Wea. Rev.,* **113,** 117–133.

Thorpe, A. J., M. J. Miller, and M. W. Moncrieff, 1982: Two-dimensional convection in nonconstant shear: A model of midlatitude squall lines. *Quart. J. Roy. Meteor. Soc.,* **108,** 739–762.

Weisman, M. L., J. B. Klemp, and R. Rotunno, 1988: Structure and evolution of numerically simulated squall lines. *J. Atmos. Sci.,* **45,** 1990–2013.